Performance analysis of a non-platinum group metal catalyst based on iron-aminoantipyrine for direct methanol fuel cells

David Sebastián[a], Vincenzo Baglio[a,*], Antonino S. Aricò[a], Alexey Serov[b] and Plamen Atanassov[b,*]

[a] *CNR-ITAE, Istituto di Tecnologie Avanzate per l'Energia "Nicola Giordano", Via Salita S. Lucia sopra Contesse 5, 98126, Messina, Italy*

[b] *Department of Chemical and Biological Engineering and Center for Micro-Engineered Materials, Farris Engineering Center, University of New Mexico, Albuquerque, NM 87131, USA*

* Corresponding authors: baglio@itae.cnr.it, plamen@unm.edu

Abstract

A highly active non-platinum group metals (non-PGMs) catalyst for oxygen reduction reaction (ORR) was synthesized by the Sacrificial Support Method (SSM) developed at the University of New Mexico (UNM). SSM was modified in order to control hydrophobicity and morphology of transition metal-nitrogen-carbon material (M-N-C). As prepared catalyst was evaluated by Scanning Electron Microscopy (SEM), Transmission Electron Microscopy (TEM) and Brunauer–Emmett–Teller (BET) methods. Electrochemical activity towards ORR and tolerance to methanol poisoning of Fe-N-C catalyst were studied by Rotating Disc Electrode (RDE). A performance analysis was carried out at the cathode of a Direct Methanol Fuel Cell (DMFC) comprising the variation of fuel concentration and temperature. A peak power density of about 50 W g^{-1} was recorded at 90°C in a wide range of methanol concentration (1-10 M). It was found that the non-PGM catalyst possesses an extraordinarily high tolerance to methanol crossover, with no significant decay of performance up to 10 M of alcohol concentration, making this material state-of-the-art in DMFC application. Chronoamperometric tests in DMFC at 90ºC and 5 M methanol concentration (100 hours) showed also a suitable stability.

Keywords: DMFC, non-PGM, ORR, electrocatalysts, M-N-C

1. Introduction

Direct methanol fuel cells (DMFCs) are considered as an attractive alternative to batteries for portable applications and auxiliary power units mainly due to advantages of low temperature liquid-fed fuel cells, such as high energy density of methanol as well as high energy efficiency [1-4].

One of the main drawbacks of DMFCs based on proton exchange membranes (PEMs) is the need of platinum group metals (PGMs) to achieve a practical performance at low temperature (< 100°C). At the moment, Pt at the cathode and PtRu at the anode are the benchmark formulations [5, 6]. Despite the fact that in the last years the catalysts composition and structure have been optimized by different approaches resulting in improvement of fuel cell performance [7-10], the cost and scarce resources of Pt still hinder the commercialization of this kind of efficient energy conversion device [11]. One attractive idea is to substitute cathodic Pt/C catalyst with recently developed highly performing non-platinum group metal (non-PGM) catalysts [12-16]. Among them, formulations based on transition metals M (where M=Fe, Co, etc.), nitrogen and carbon materials, abbreviated in literature as M-N-C, present great prospect for fuel cell application [17-24].

The development of mentioned above non-PGM catalysts was targeted on implementation into H_2/O_2 PEMFCs and only a few papers deal with utilization of M-N-Cs in DMFCs configuration. Up to date, some published results with different non-PGM formulations can be considered as promising, the difference in membrane-electrode assemblies (MEAs) fabrication, cell operating conditions and cells hardware does not allow directly comparing them. For instance, B. Piela et al. reported 45 mW cm^{-2} with a Co-based catalyst derived from tetramethoxyphenylporphyrin precursor with a loading of 2 mg cm^{-2} at the cathode, and 6 mg cm^{-2} of PtRu at the anode, operating at 70°C, 1.1 M methanol and pressurized air (2.04 atmg) [25]. Y. Wei et al. obtained 58 mW cm^{-2} employing 10 mg cm^{-2} Fe catalyst supported on N-doped carbon aerogel at the cathode and 4 mg cm^{-2} PtRu at the anode, operating at 60°C with 2 M methanol and oxygen [26]. Y. Hu et al. have

very recently reported a peak power of 21 mW cm^{-2} for a polyaniline-derived Fe-N-C doped with phosphorous, with 4 mg cm^{-2} at the cathode and 1.5 mg cm^{-2} PtRu at the anode, operating at 50°C, 2 M methanol and oxygen [27]. E. Negro et al. have recently reported Fe-N supported on graphitic carbon nano-networks with a loading of 2.5 mg cm^{-2} at the cathode, and 2.5 mg cm^{-2} PtRu at the anode, obtaining 15 mW cm^{-2} at 90°C with 2 M methanol and oxygen [28]. As a general observation, the decrease of catalyst loading results in lower performances; however, platinum content reduction or full elimination is mandatory towards cost-effective DMFC systems.

The main objective of the present work is to investigate the performance of PEM-DMFC based on a non-PGM cathode catalyst derived from pyrolysis of iron aminoantipyrine (Fe-AAPyr). In this class of catalysts, the covalent integration of Fe-N_x sites into π-conjugated carbon basal planes modifies the carbonaceous ligand capability of donating/withdrawing electrons, resulting in reasonably high oxygen reduction reaction (ORR) activity [29]. This catalyst has already been proven to be a perspective for the ORR in rotating disk characterization [30] and, more recently, very promising results have been obtained in the application at the cathode of alkaline direct methanol fuel cells [31]. Up to know, the performance of this class of non-PGM catalysts in PEM-based DMFCs has not been evaluated. Herein, the influence of cathode loading, cell operating temperature and methanol concentration on the electrochemical behavior has been investigated, employing a low PtRu loading at the anode in order to derive the performance for cost-effective and practical DMFC systems.

2. Experimental

2.1. Materials preparation and physico-chemical characterization

Non-PGM Fe-AAPyr catalysts was synthesized by substantially modified Sacrificial Support method (SSM), developed at UNM [24, 29, 32, 33]. Initially calculated amount of low surface area

fumed silica (L90, Cab-O-Sil®, Cabot, surface area ~90 m^2 g^{-1}) was mixed with $Fe(NO_3)_3 \cdot 9H_2O$ (Sigma Aldrich) and 4-Aminoantipyrine (AAPyr, Sigma Aldrich) and in-house made carbon nanotubes (CNTs) [34]. Obtained mixture was subjected to dry mechanochemical treatment [35] by ball-milling in planetary ball mill at 400 rpm for 1 hour. The finely homogenized mixture of precursors was pyrolized in inert atmosphere of Ultra High Purity (UHP) nitrogen at flow rate of 100 mL min^{-1}, 975°C and 45 minutes. Sacrificial support was removed by means of 25wt% of HF for 48 hours. Powder was washed with deionized water until neutral pH. In order to remove un-washed volatile silica compounds, a second treatment in ammonia atmosphere was carried out at 1000°C and 25 min. As obtained Fe-AAPyr catalyst was used in present study. Scanning electron microscopy (SEM) and transmission electron microscopy (TEM) images were obtained using Hitachi S-800 and JEOL 2010 EX instruments, respectively. Surface areas were measured by N_2 adsorption BET using a Micrometrics 2360 Gemini Analyzer. A four-point BET analysis was performed using a saturation pressure of 640 mmHg.

2.2. Half-cell characterization

Electrochemical studies were carried out in a three-electrode cell at room temperature. 0.5 M H_2SO_4 was used as electrolyte, the reference electrode was a mercury/mercury sulfate ($Hg|Hg_2SO_4$, sat. K_2SO_4) electrode and a high surface Pt coiled wire was used as counter electrode. A rotating disk electrode (RDE) consisting of a thin film catalyst deposited on the glassy carbon disk (5 mm) was used as working electrode (WE). The catalytic layer was obtained following this recipe: first preparing 3 mg mL^{-1} ink by sonicating the catalyst in isopropyl alcohol/water (3/1, v/v) solution and Nafion® (Ion Power, 5 wt%). Some drops of this ink were deposited onto the glassy carbon disk to reach the desired mass loading (0.6 mg cm^{-2} for the Fe-AAPyr catalyst, 15 wt% Nafion® according to previous works [29]. An Autolab potentionstat/galvanostat was used to carry out the electrochemical experiments. Linear sweep voltammetry curves were carried out in the potentiostatic mode with a scan rate of 5 mV s^{-1} and at rotation rates from 100 rpm to 2500 rpm.

The tolerance of the catalysts to the presence of methanol was evaluated by adding increasing aliquots of the alcohol to the base electrolyte, saturated with oxygen, for concentrations from 0.005 M to 2 M. The ORR response in the presence of methanol was evaluated at a rotation speed of 1600 rpm.

2.3. Fuel cell testing

Cathode electrodes were prepared by spraying a catalytic ink on a commercial hydrophobic gas diffusion layer (GDL-LT, E-TEK). The catalyst ink was prepared sonicating the catalyst in an isopropyl alcohol/water mixture (2/1, v/v) and Nafion® solution. The Nafion® content in the catalytic layer was 45 wt% [24]. Electrodes were prepared using the non-PGM catalyst (Fe-AAPyr) with loading values of 2.7 mg cm^{-2} and 7.4 mg cm^{-2}. For comparison purposes, a cathode based on commercial 40 wt% Pt/C (Johnson Matthey) was prepared following the same spraying procedure (1 mg Pt cm^{-2}, 33 wt% Nafion®) [36]. Anode electrodes based on PtRu black (Pt:Ru 1:1, Johnson Matthey) were prepared by doctor blade according to the procedure described in a previous report [37]. The catalytic layer was composed of 85 wt% catalyst and 15 wt% Nafion® ionomer, spread onto a commercial gas diffusion layer (GDL-HT, E-TEK). The noble metal (Pt+Ru) loading at the anode was 1 mg cm^{-2} in all membrane-electrode assemblies (MEAs).

MEAs were formed by a hot-pressing procedure at 130 °C and 30 kgf cm^{-2} during 10 minutes, and subsequently installed in a 5 cm^2 fuel cell test fixture (Fuel Cell Tech., Inc.). A Nafion® 115 membrane (~130 µm) was used as the solid electrolyte. In the various MEAs, the anode loading was maintained constant (PtRu black Johnson Matthey, 1 mg PtRu cm^{-2}) whereas the cathode loading was varied. The cell hardware was connected to a Fuel Cell Tech., Inc. test station. In case of single cell polarization experiments, aqueous methanol (from 1 M to 10 M) was pre-heated at the same temperature of the cell and fed to the anode chamber of the DMFC through a peristaltic pump; oxygen, pre-heated at the same temperature of the cell (100% relative humidity), was fed to the cathode. Reactant flow rates were 2 and 100 mL min^{-1} for methanol/water mixture and oxygen

stream, respectively. The cell temperature was measured by a thermocouple embedded in the cathodic graphite plate, close to the MEA. Steady-state galvanostatic polarization experiments in DMFC were performed with an Agilent electronic load at various temperature and methanol concentration conditions. An Agilent milliohmeter operating at 1 kHz was used to determine the resistance of the cell. In order to evaluate the methanol cross-over, chromatographic analyses at the cathode exhaust were carried out and the CO_2 concentration was determined by quantification of the CO_2 peak area. The MEA based on the platinum cathode was used for this determination and complete oxidation of permeated methanol to CO_2 was assumed.

A 100 h chronoamperometric experiment at 0.3 V was carried out to evaluate the stability of the MEA based on the most performing non-PGM formulation (Fe-AAPyr 7.4). Cell conditions were 90 °C, 5 M methanol fed to the anode and humidified O_2 fed to the cathode (2 and 100 mL min^{-1} respectively). The performance was evaluated by means of steady-state galvanostatic polarization curves under identical conditions to those reported above.

3. Results and discussion

3.1. Catalyst characterization

As it was mentioned, the SSM assisted by mechanochemical treatment was modified in order to synthesize catalyst for DMFC application. It is well-known that mass-transfer limitations on the cathode side of MEA may result in substantial decrease in overall performance. One of the possible mechanisms of such limitation is flooding, which affects on the accessibility of catalyst active sites. ORR itself produces water which potentially can flood the cathode catalyst. In the DMFCs, the case is even more complicated due to the fact that substantial amount of methanol crossovers through the membrane and induces additional flooding. In order to mitigate this drawback, hydrophobicity and morphology of catalyst should be improved. In UNM previous works it was shown that Fe-AAPyr

prepared by conventional SSM has surface area around 1000 m^2 g^{-1} with mainly pores in the range of 5-10 nm [30]. Such pores can be easily flooded by combination of water from ORR and methanol from crossover processes. In the present study, we modified SSM by using low surface area sacrificial support and addition of CNTs. The usage of 90 m^2 g^{-1} silica results in increase of pore size (surface area of final material was decreased to 450 m^2 g^{-1}), while usage of 100% graphitic CNTs leads to increase of level of hydrophobicity. As it can be seen from Figure 1, Fe-AAPyr material possesses combination of open-framed structure as well as CNTs features.

3.2. Tolerance to methanol poisoning, half-cell tests

One of the most desirable characteristics for a cathode catalyst in a DMFC is a high tolerance to the presence of methanol [38-42]. Some encouraging results have been already published regarding this aspect for non-PGM catalysts [25]. This property is ascribed to the intrinsic inactivity towards methanol electro-oxidation of such catalysts while presenting a high activity towards the ORR. Figure 2 shows linear sweep voltammetry curves towards ORR in the presence of various methanol concentrations (from 5 mM to 2 M) in sulfuric acid electrolyte (0.5 M H_2SO_4), obtained for the Fe-AAPyr catalyst in RDE. A detailed electrochemical analysis of this family of Fe-based catalyst towards the ORR in the absence of methanol can be referred to previous works [29, 30, 32]. A remarkable tolerance to the presence of methanol was observed for the Fe-AAPyr catalyst as it can be clearly seen in Figure 2. Even at a methanol concentration as high as 2 M, oxygen reduction process takes place without any evidence of alcohol oxidation. There is only a slight shift of the curve towards more negative potentials compared to the curve without methanol. The half-wave potential ($E_{1/2}$, i.e. the potential when the current is half of the diffusion limiting current, $i_d/2$) changes only 8 mV at 5 mM CH_3OH and 16 mV at 2 M CH_3OH with respect to the curve without methanol. The behavior of $E_{1/2}$ shift with methanol concentration is not linear; i.e. passing from 0 to 5 mM methanol the potential varies -8 mV and passing from 5 mM to 2 M the shift is also -8 mV. In other words, analyzing the ORR activity in the mixed kinetic-diffusion controlled region, the

presence of 0.01 M methanol causes a decrease in current of only 7%. Passing from 0.01 M to 0.1 M (one order of magnitude) results in a decrease of 3%, whereas from 0.1 M to 1 M, the current decay is only 2%. Thus, the very small variation of current with the large increase of methanol concentration suggests that there could be a very weak interaction between methanol and ORR active sites (negligible adsorption), or that only a small fraction of active sites may be affected by methanol poisoning. In a conventional Pt/C catalyst, the effect of methanol on the ORR activity is much more pronounced. The $E_{1/2}$ potential decreases up to 50 mV in the presence of small concentration of methanol (5 mM) [43]. At methanol concentrations higher than 50 mM, oxidation currents are observed, resulting in a shift of $E_{1/2}$ as high as 200 mV towards more negative potentials for 0.5 M methanol concentration [43]. These results represent a clear evidence of the high methanol tolerance demonstrated by the Fe-AAPyr catalyst.

3.3. Direct methanol fuel cell tests of Fe-AAPyr catalyst

In this section, the performance of the non-PGM cathode catalyst based on iron aminoantipyrine (Fe-AAPyr) is analyzed in a single cell fed with methanol and oxygen. The study consists of the variation of temperature (30-90°C) and methanol concentration (1-10 M). In a DMFC system, the required volume of the fuel reservoir tremendously depends on the methanol concentration. Table 1 summarizes the energy density of methanol aqueous solutions as a function of concentration to better illustrate (quantitatively) the connection between both parameters. The main advantage of using high methanol concentration is related to a prolonged operation of DMFC-based systems. On the other side, the main disadvantage of high methanol concentration at the anode is the loss of electrical efficiency due to the crossover effect in conventional cells based on Pt cathode. Increasing the methanol concentration at the anode leads to the increase of the diffusion gradient of the alcohol through the polymeric proton conductive membrane. Moreover, temperature favors the diffusivity of methanol; thus, both variables (temperature and concentration) influence the rate of methanol permeation. This is illustrated in Table 2 for a Nafion® 115 membrane, where data of methanol

cross-over rate (in μmol cm^{-2} min^{-1}) are reported. The methanol cross-over was determined by the analysis of the CO_2 produced at the cathode assuming the complete oxidation of permeated methanol in the presence of Pt catalyst at open circuit potential (OCP) condition for the standard MEA (Pt-based cathode). The presence of methanol at the cathode creates a mixed potential in conventional cathodes based on Pt, which diminishes the overall efficiency of state-of-the-art MEAs.

Polarization and power density curves obtained at 30°C for the cell configuration based on Fe-AAPyr as cathode are shown in Figure 3, in which the effect of methanol concentration is studied. Two different Fe-AAPyr loadings were tested as described in the experimental section: 2.7 mg cm^{-2} (Figure 3a) and 7.4 mg cm^{-2} (Figure 3b). For comparison purposes, Figure 3c shows the DMFC tests obtained under identical conditions using a commercial Pt/C catalyst at the cathode (1 mg Pt cm^{-2}). The detrimental effect of methanol for Pt-based cathode is clearly visible in Figure 3c, especially at low current, where the potential significantly decreases with the increase of methanol concentration. It is remarkable that for the Fe-AAPyr cathode, regardless the methanol concentration, the polarization curves present the same potential-current behavior in the activation controlled region, i.e. at low current density (Figs. 3a,b). This effect is also independent of Fe-AAPyr loading. The high methanol tolerance properties of such Fe-AAPyr catalyst, as evidenced in the half-cell characterization, is also demonstrated by these polarization curves, which show a similar behavior in the wide range of methanol concentrations investigated. Another remarkable result regarding methanol tolerance is that the OCP is barely modified with the increase of methanol concentration for the Fe-AAPyr catalyst (only 10 mV decrease). Whereas, for the reference MEA based on Pt, the decay amounts to 60 mV. The variation of OCP values with cell conditions and the type and loading of cathode catalyst will be further discussed in a subsequent section.

At high current density, the polarization curves for the non-PGM cathode show increasing performance with the increase of methanol concentration, showing the maximum power density at

30°C of 6.5 mW cm^{-2} in the case of 7.4 mg cm^{-2} Fe-AAPyr cathode. There is only a slight decrease of performance passing from 5 M to 10 M methanol concentration (< 5%). On the other hand, the MEA based on Pt cathode achieves a power density of 11.1 mW cm^{-2} feeding 2 M methanol; whereas, at 10 M methanol the performance decreases to 9.1 mW cm^{-2} due to the cross-over effect (-18%).

In a similar way, polarization and power density curves obtained at 60°C are shown in Figure 4. Analogous discussion of the effect of methanol concentration can be applied at this temperature. However, higher temperature leads to the increase of electrode kinetics (both anodic and cathodic) and membrane ionic conductivity, both contributing to an increase of overall performance. The resistance of the cell (R) is reported at different temperatures in Table 2. It is clear that R decreases with temperature as a result of the increase of ionic (protonic) conductivity of Nafion®. However, the raise of temperature increases also methanol permeation through the polymer electrolyte (Table 2), and as a consequence, the cross-over effect becomes more detrimental to the cell performance.

At 60°C the voltage decay in the activation controlled region (i.e. at low current density) amounts to about 250 and 300 mV for the Fe-AAPyr-based cathodes, Figs 4b and 4a, respectively. Such voltage decay for this type of non-PGM catalysts is independent of methanol concentration, variable that presents only a significant influence in the high current density region. This is more evident in Fig 4b, where the highest methanol concentration tested favors the highest power output. Whereas, the voltage decay for the Pt-based cathode amounts to ca. 400 mV in the case of high methanol concentration at the anode (10 M). The differences between Pt and Fe-AAPyr in methanol tolerance are also evidenced by the variation of OCP when passing from 1M to 10M methanol, as in the case of experiments at low temperature. The decrease of OCP amounts to 20-45 mV in the case of Fe-AAPyr cathodes, and about 120 mV in the case of Pt-cathode.

The maximum peak power density for the non-PGM formulation at 60°C was 18 mW cm^{-2}, obtained with high concentration of methanol (either 5 M or 10 M) and the high loaded cathode (7.4

mg cm^{-2} Fe-AAPyr). This performance is yet low but it must be considered that a low Pt loading is used at the anode (0.7 mg Pt cm^{-2}). Usually, a linear increase of performance is recorded with the Pt loading from 1 mg cm^{-2} to 5 mg cm^{-2}, range commonly found in the literature for DMFC applications [5, 44]. However, a low Pt loading is required towards cost-effective DMFC systems. The gap in performance between the MEAs based on Fe-AAPyr and that on Pt is reduced when 10 M methanol is fed to the anode; under this condition, the methanol tolerance of the non-PGM formulation plays a favoring role in maintaining the same power density with the increase of methanol concentration.

DMFC performance curves obtained at 90°C are shown in Figure 5. The cross-over of methanol increases at high temperature (Table 2), as well as the membrane conductivity (Table 2) and electrode kinetics. The Fe-AAPyr-based MEAs (Figs 5a and 5b) present a similar voltage-current behavior at 90°C than at lower temperatures (30°C and 60°C) but are characterized by higher performances. Again, a negligible effect of methanol concentration at the anode is obtained in the activated controlled region, where the potential decay amounts to about 300 mV regardless the methanol concentration at the anode. The OCP decay when passing from 1 M to 10 M methanol is about 25-35 mV, which is similar to those obtained at lower temperatures. It appears that there is not any influence of neither temperature nor catalyst loading on the OCP. Instead, the MEA based on Pt/C cathode shows a considerable voltage decay at low current density with the increase of methanol concentration at the anode. In this case, the OCP decreases 280 mV when passing from 1 M to 10 M methanol. The voltage drop at low current density is about 500 mV for the cell fed with 10 M methanol, highlighting the very detrimental effect of methanol cross-over on the electrical efficiency of a DMFC based on Pt cathode.

Figure 6 shows the dependence of the cell current at 0.2 V on the methanol concentration fed to the anode side for the three investigated MEAs. Regardless the temperature, the MEAs based on the Fe-AAPyr catalyst present no significant variation of current density with methanol concentration.

In contrast, the MEA based on Pt/C presents a significant decay of current with methanol concentration, approaching the values obtained with the non-PGM cathode at 10 M methanol. This is a clear indication of the tolerance to permeated methanol for the herein studied non-PGM formulation based on Fe-AAPyr.

The OCP values at different cell conditions for the investigated MEAs are shown in the bar graph of Figure 7. It is known that OCP increases with cell temperature and oxygen pressure but decreases with methanol concentration. Regardless the loading, the cathodes based on Fe-AAPyr catalyst present OCP values in the range 0.7-0.8 V, mostly influenced by temperature. In fact, it is remarkable that only slight changes in OCP values are observed when increasing methanol concentration at the anode. On the other hand, the Pt-based cathode experiences a significant decrease of OCP with the increase of methanol concentration. This potential decay with methanol concentration for the Pt-based cathode is especially dramatic at 90 °C, where OCP is 0.78 V for 1 M CH_3OH and 0.50 V for 10 M CH_3OH (loss of 280 mV), whereas in equivalent conditions, the Fe-AAPyr varies only 30 mV. Slightly lower values of OCP for the high-loaded Fe-AAPyr cathode are also observed in comparison to the low-loaded one. The thicker the electrode the slower the transport phenomena at the catalytic layer (including mass transport, electron transport, etc.), which may lead to slight differences in charge transfer phenomena at open circuit. Taking into account that the only difference between the Fe-AAPyr electrodes is thickness, this may explain the slightly higher OCP values for the thinnest electrode (2.7 mg cm^{-2}).

3.4. Comparative study of performance and cost-effectiveness

The cost-effectiveness of the Fe-AAPyr catalysts was analyzed normalizing the cell polarization curves by the MEA total platinum content, assuming that the main contribution to the electrode cost is the platinum total weight content (ruthenium is about one order of magnitude cheaper than platinum, and the non-PGM catalyst costs about two orders of magnitude less than Pt). The MEAs based on the Fe-AAPyr cathode contain 0.67 mg Pt cm^{-2} (1 mg PtRu cm^{-2}, Pt:Ru = 1:1 at.), whereas

the MEA based on Pt-cathode contains 1.67 mg cm^{-2} (0.67 mg Pt cm^{-2} at the anode and 1 mg Pt cm^{-2} at the cathode). Normalized polarization and power density curves are shown in Figure 8 feeding 10 M methanol to the anode. At low temperature (30°C), a low Fe-AAPyr loading is enough to outperform a Pt-cathode-based MEA in terms of performance-to-cost. At 60°C and 90°C, the low loading Fe-AAPyr cathode shows comparable results to the Pt-based cathode. At temperatures higher than ambient, higher Fe-AAPyr loadings are preferable in terms of normalized power output reaching about 45 W $g^{-1}_{Pt\text{-}MEA}$. Furthermore, as already evidenced before, the non-PGM catalyst allows an increase of potential at low current densities, using high methanol concentration, compared to Pt due to better methanol tolerance properties of the Fe-AAPyr.

The optimum non-PGM catalyst content depends on the application of the fuel cell, which defines working conditions such as temperature and fuel concentration. Figure 9 summarizes the normalized peak power density as a function of the operating conditions in order to individuate the best cathode formulation for a specific application. For instance, at low temperatures (30-60°C), as in the case of portable applications, the best configuration appears to be the high-loading Fe-AAPyr regardless the methanol concentration; whereas, at high temperature, as in the case of auxiliary power units, the best choice depends on the methanol concentration, but to maximize the energy density a high methanol concentration is preferable; thus, the Fe-AAPyr cathode seems to be the best approach.

3.5. Stability of Fe-AAPyr based MEA

The long-term stability in the DMFC acidic environment still represents a major challenge for the introduction and development of cathodic non-PGM catalysts. A stability test was performed on the Fe-AAPyr7.4-based MEA as shown in Figure 10a. The current density was collected at a constant voltage of 0.3 V for 100 hours, operating at 90°C, 5M methanol at the anode and humidified oxygen at the cathode. A polarization curve was recorded every 10 hours to evaluate the performance variation with time (indicated in the figure). The major decrease of current is

registered within the first 3 hours, passing from 70 mA cm^{-2} at the beginning of life (BoL) to about 50 mA cm^{-2} (decay rate of about 6.3 mA cm^{-2} h^{-1}). Afterwards, the current decay is slowed down to about 0.2-0.3 mA cm^{-2} h^{-1}. After every polarization curve, a part of the current density is recovered (about 15%), as indicated by a slight increase of current every 10 hours. An increase of current density was also observed after test interruptions occurred at 47 and 78 hours. The recovery of a part of the current indicates that the loss of performance presents reversible and irreversible contributions.

Figure 10b shows the DMFC performance at BoL, after 50 hours operation and at the end of the stability test (EoT, 100 h). The peak power density suffers a decrease from about 35 mW cm^{-2} to 15 mW cm^{-2} in the whole period of the experiment, although the major decay occurs within the first hours of operation, 23 mW cm^{-2} after 50 h, as also observed in Figure 10a. For prolonged operation, the current decay slows down and the performance loss decelerates with time, as is also envisaged from the comparison of the three polarization curves in Figure 10b.

4. Conclusions

A highly active oxygen reduction cathode catalyst from the family of non-PGM materials was synthesized by modified Sacrificial Support Method assisted by mechanochemical approach. This catalyst was evaluated by SEM, TEM, BET and electrochemical methods and it was shown that modification in preparation method affected on its morphology and surface properties. The results of electrochemical characterization by RDE and fuel cell tests revealed that Fe-AAPyr catalyst has one of the highest methanol tolerance reported in the open literature, not substantial fuel cell performance drop was observed up to methanol concentration of 10 M. Stability test at 90ºC and 5M methanol showed a slow decrease of performance with time. Such promising results place mentioned above Fe-AAPyr catalyst into the category of state-of-the-art DMFC ORR materials.

Taking into account that Fe-AAPyr cost is two orders of magnitude lower compared to platinum this catalyst can be used as highly active, methanol tolerant and inexpensive substitute of platinum in DMFCs systems.

Acknowledgments

CNR-ITAE authors acknowledge the financial support of PRIN2010-11 project 'Advanced nanocomposite membranes and innovative electrocatalysts for durable polymer electrolyte membrane fuel cells' (NAMED-PEM).

References

[1] N. Kimiaie, K. Wedlich, M. Hehemann, R. Lambertz, M. Müller, C. Korte, D. Stolten, Energy Environ. Sci. 7 (2014) 3013-3025.

[2] J.N. Tiwari, R.N. Tiwari, G. Singh, K.S. Kim, Nano Energy 2 (2013) 553–578.

[3] A.S. Aricò, V. Baglio, V. Antonucci, in: H. Liu, J. Zhang (Eds.), Electrocatalysis of Direct Methanol Fuel Cells, WILEY-VCH Verlag GmbH & Co. KGaA, Weinheim, 2009, pp. 1-78.

[4] A. Serov, C. Kwak, Appl. Catal. B: Environ. 90 (2009) 313-320.

[5] A. Brouzgou, S.Q. Song, P. Tsiakaras, Appl. Catal. B: Environ. 127 (2012) 371–388.

[6] X. Zhao, M. Yin, L. Ma, L. Liang, C. Liu, J. Liao, T. Lu, W. Xing, Energy Environ. Sci. 4 (2011) 2736-2753.

[7] C. Alegre, M.E. Gálvez, R. Moliner, V. Baglio, A.S. Aricò, M.J. Lázaro, Appl. Catal. B: Environ. 147 (2014) 947– 957.

[8] S. Basri, S.K. Kamarudin, W.R.W. Daud, Z. Yaakub, Int. J. Hydrogen Energy 35 (2010) 7957-7970.

[9] K. Wang, Y. Wang, Z. Liang, Y. Liang, D. Wu, S. Song, P. Tsiakaras, Appl. Catal. B: Environ. 147 (2014) 518-525.

[10] E. Antolini, T. Lopes, E.R. Gonzalez, J. Alloys Compd. 461 (2008) 253–262.

[11] F. Jaouen, E. Proietti, M. Lefèvre, R. Chenitz, J.P. Dodelet, G. Wu, H.T. Chung, C.M. Johnston, P. Zelenay, Energy Environ. Sci. 4 (2011) 114-130.

[12] D. Zhao, J.L. Shui, C. Chen, X. Chen, B.M. Reprogle, D. Wang, D.J. Liu, Chem. Sci., 3 (2012) 3200-3205.

[13] G. Wu, K.L. More, C.M. Johnston, P. Zelenay, Science, 332 (2011) 443-447.

[14] A. Ishihara, Y. Ohgi, K. Matsuzawa, S. Mitsushima, K.I. Ota, Electrochim. Acta 55 (2010) 8005–8012.

[15] K. Strickland, E. Miner, Q. Jia, U. Tylus, N. Ramaswamy, W. Liang, M.T. Sougrati, F. Jaouen, S. Mukerjee, Nat. Commun. 6 (2015) 7343.

[16] K. Wan, G.F. Long, M.Y. Liu, L. Du, Z.X. Liang, P. Tsiakaras, Appl. Catal. B: Environ. 165 (2015) 566-571.

[17] Y. Hu, J.O. Jensen, W. Zhang, L.N. Cleemann, W. Xing, N.J. Bjerrum, Q. Li, Angew. Chem. Int. Ed. 53 (2014) 3675-3679.

[18] F. Jaouen, V. Goellner, M. Lefèvre, J. Herranz, E. Proietti, J.P. Dodelet, Electrochim. Acta 87 (2013) 619-628.

[19] E. Proietti, F. Jaouen, M. Lefèvre, N. Larouche, J. Tian, J. Herranz, J.P. Dodelet, Nature Commun. 2 (2011) 416.

[20] U.I. Kramm, J. Herranz, N. Larouche, T.M. Arruda, M. Lefèvre, F. Jaouen, P. Bogdano, S. Fiechter, I. Abs-Wurmbach, S. Mukerjee, J.P. Dodelet, Phys. Chem. Chem. Phys. 14 (2012) 11673-11688.

[21] F. Jaouen, J. Herranz, M. Lefèvre, J.P. Dodelet, U.I. Kramm, I. Herrmann, P. Bogdanoff, J. Maruyama, T. Nagaoka, A. Garsuch, J.R. Dahn, T. Olson, S. Pylypenko, P. Atanassov, E.A. Ustinov, ACS Appl. Mater. Interfaces 1 (2009) 1623-1639.

[22] A.H.A. Monteverde Videla, L. Zhang, J. Kim, J. Zeng, C. Francia, J. Zhang, S. Specchia, J. Appl. Electrochem. 43 (2013) 159-169.

[23] A.H.A. Monteverde Videla, S. Ban, S. Specchia, L. Zhang, J. Zhang, Carbon 76 (2014) 386-400.

[24] A. Serov, K. Artyushkova, P. Atanassov, Adv. Energy Mater. 4 (2014) 1301735.

[25] B. Piela, T.S. Olson, P. Atanassov, P. Zelenay, Electrochim. Acta 55 (2010) 7615-7621.

[26] Y. Wei, C. Shengzhou, L. Weiming, Int. J. Hydrogen Energy 37 (2012) 942-945.

[27] Y. Hu, J. Zhu, Q. Lv, C. Liu, Q. Li, W. Xing, Electrochim. Acta 155 (2015) 335-340.

[28] E. Negro, A.H.A. Monteverde Videla, V. Baglio, A.S. Aricò, S. Specchia, G.J.M. Koper, Appl. Catal. B: Environ. 166-167 (2015) 75-83.

[29] U. Tylus, Q. Jia, K. Strickland, N. Ramaswamy, A. Serov, P. Atanassov, S. Mukerjee, J. Phys. Chem. C 118 (2014) 8999-9008.

[30] A. Serov, M.H. Robson, B. Halevi, K. Artyushkova, P. Atanassov, Electrochem. Commun. 22 (2012) 53-56.

[31] R. Janarthanan, A. Serov, S.K. Pilli, D.A. Gamarra, P. Atanassov, M.R. Hibbs, A.M. Herring, Electrochim. Acta (2015) doi: 10.1016/j.electacta.2015.03.209.

[32] A. Serov, M. H. Robson, M. Smolnik, P. Atanassov, Electrochim. Acta 109 (2013) 433-439.

[33] A. Serov, A. Aziznia, P. H. Benhangi, K. Artyushkova, P. Atanassov, E. Gyenge, J. Mater. Chem. A 1 (2013) 14384-14391.

[34] N. I. Andersen, A. Serov, P. Atanassov, Appl. Catal. B: Environ. 163 (2015) 623-627.

[35] A. Serov, K. Artyushkova, N. I. Andersen, S. Stariha, P. Atanassov, Electrochim. Acta (2015) doi:10.1016/j.electacta.2015.02.108.

[36] V. Baglio, A. Di Blasi, A.S. Aricò, V. Antonucci, P.L. Antonucci, F. Nannetti, V. Tricoli, Electrochim. Acta 50 (2005) 5181-5188.

[37] A.S. Aricò, A. Stassi, C. D'Urso, D. Sebastián, V. Baglio, Chem. A Eur. J. 20 (2014) 10679-10684.

[38] M. Asteazaran, S. Bengió, W.E. Triaca, A.M. Castro Luna, J. Appl. Electrochem. 44 (2014) 1271-1278.

[39] W. Li, X. Zhao, T. Cochell, A. Manthiram, Appl. Catal. B: Environ., 129 (2013) 426-436.

[40] G. Selvarani, S. Maheswari, P. Sridhar, S. Pitchumani, A.K. Shukla, J. Electrochem. Soc. 156 (2009) B1354-B1360.

[41] C. Lamy, C. Coutanceau, N. Alonso-Vante, in: H. Liu, J. Zhang (Eds.), Electrocatalysis of Direct Methanol Fuel Cells, WILEY-VCH Verlag GmbH & Co. KGaA, Weinheim, 2009, pp. 257-314.

[42] H. Yang, C. Coutanceau, J.M. Léger, N. Alonso-Vante, C. Lamy, J. Electroanal. Chem. 576 (2005) 305-313.

[43] D. Sebastián, V. Baglio, S. Sun, A.C. Tavares, A.S. Aricò, ChemCatChem 7 (2015) 911-915.

[44] V. Baglio, A. Di Blasi, E. Modica, P. Cretì, V. Antonucci, A.S. Aricò, Int. J. Electrochem. Sci. 1 (2006) 71-79.

Table 1. Energy density of methanol aqueous solutions as a function of methanol concentration.

Methanol concentration mol L^{-1}	Methanol percentage wt%	Energy density Wh g^{-1}
1	3.2	195
2	6.4	393
5	16.5	1007
10	34.5	2106

Table 2. DMFC operating parameters: resistance (R) and methanol cross-over

Cell temperature °C	Resistance Ω cm^2	CH_3OH (1M)* cross-over[a] µmol cm^{-2} min^{-1}	CH_3OH (5M)* cross-over[b] µmol cm^{-2} min^{-1}
30	0.215	3.5	15.4
60	0.166	10.7	47.9
90	0.138	31.7	76.8

* CH_3OH concentration fed to the anode.

Captions to figures

Figure 1. SEM (a) and TEM (b) images of Fe-AAPyr hybrid with CNTs catalyst.

Figure 2. ORR linear sweep voltammetric curves in RDE, O_2-saturated 0.5 M H_2SO_4 electrolyte with different methanol (CH_3OH) concentrations. Fe-AAPyr catalyst (600 µg cm^{-2}), room temperature, rotation speed 1600 rpm, scan rate 5 mV s^{-1}.

Figure 3. DMFC performances at 30°C of (a) Fe-AAPyr 2.7 mg cm^{-2}; (b) Fe-AAPyr 7.4 mg cm^{-2}; (c) Pt/C 1 mg Pt cm^{-2}. Polarization curves (open symbols) and power density curves (closed symbols)

Figure 4. DMFC performances at 60°C of (a) Fe-AAPyr 2.7 mg cm^{-2}; (b) Fe-AAPyr 7.4 mg cm^{-2}; (c) Pt/C 1 mg Pt cm^{-2}. Polarization curves (open symbols) and power density curves (closed symbols)

Figure 5. DMFC performances at 90°C of (a) Fe-AAPyr 2.7 mg cm^{-2}; (b) Fe-AAPyr 7.4 mg cm^{-2}; (c) Pt/C 1 mg Pt cm^{-2}. Polarization curves (open symbols) and power density curves (closed symbols)

Figure 6. Dependence of the cell current density at 0.2 V on the methanol concentration for the different MEAs at 30ºC and 90ºC.

Figure 7. Open circuit potential values for the MEAs based on different cathode formulations according to the cell temperature and anode methanol concentration conditions.

Figure 8. Normalized DMFC performances at (a) 30°C; (b) 60°C; and (c) 90°C. Polarization curves (open symbols) and power density curves (closed symbols)

Figure 9. DMFC performances in terms of normalized maximum power density (W g_{Pt}^{-1}) as a function of cell operating temperature and methanol concentration.

Figure 10. (a) DMFC stability test at 0.3 V and (b) polarization and power density curves on the MEA based on Fe-AAPyr 7.4 mg cm^{-2} at the cathode and 1.0 mg PtRu cm^{-2} at the anode. Cell conditions: 90 °C, 5 M methanol and humidified oxygen (100% RH) at flow rates of 2 and 100 mL min^{-1}, respectively.

Figures

Figure 1

a) 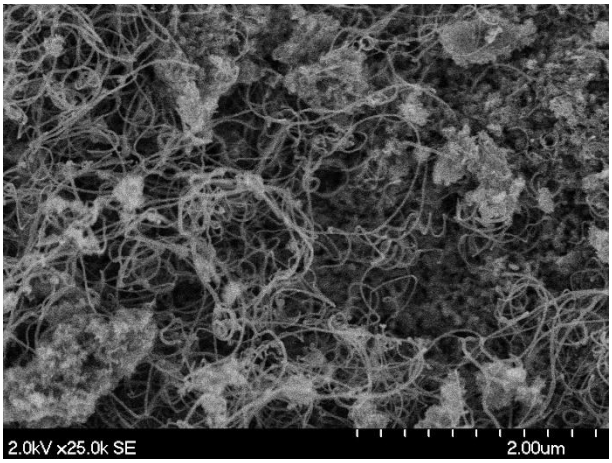

b) 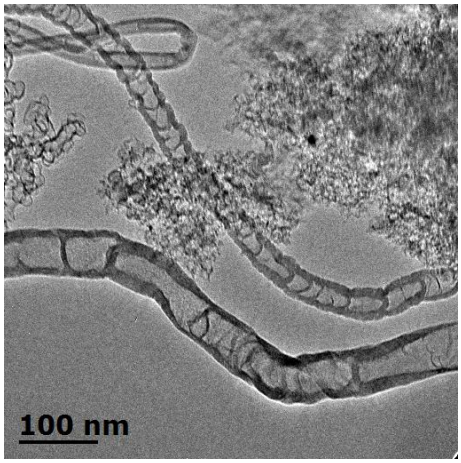

Figure 2

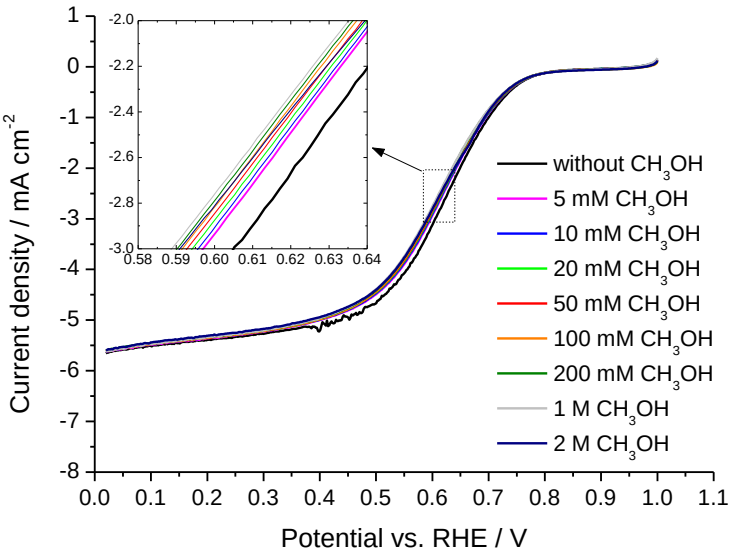
Current density / mA cm-2
Potential vs. RHE / V
without CH3OH
5 mM CH3OH
10 mM CH3OH
20 mM CH3OH
50 mM CH3OH
100 mM CH3OH
200 mM CH3OH
1 M CH3OH
2 M CH3OH

Figure 3

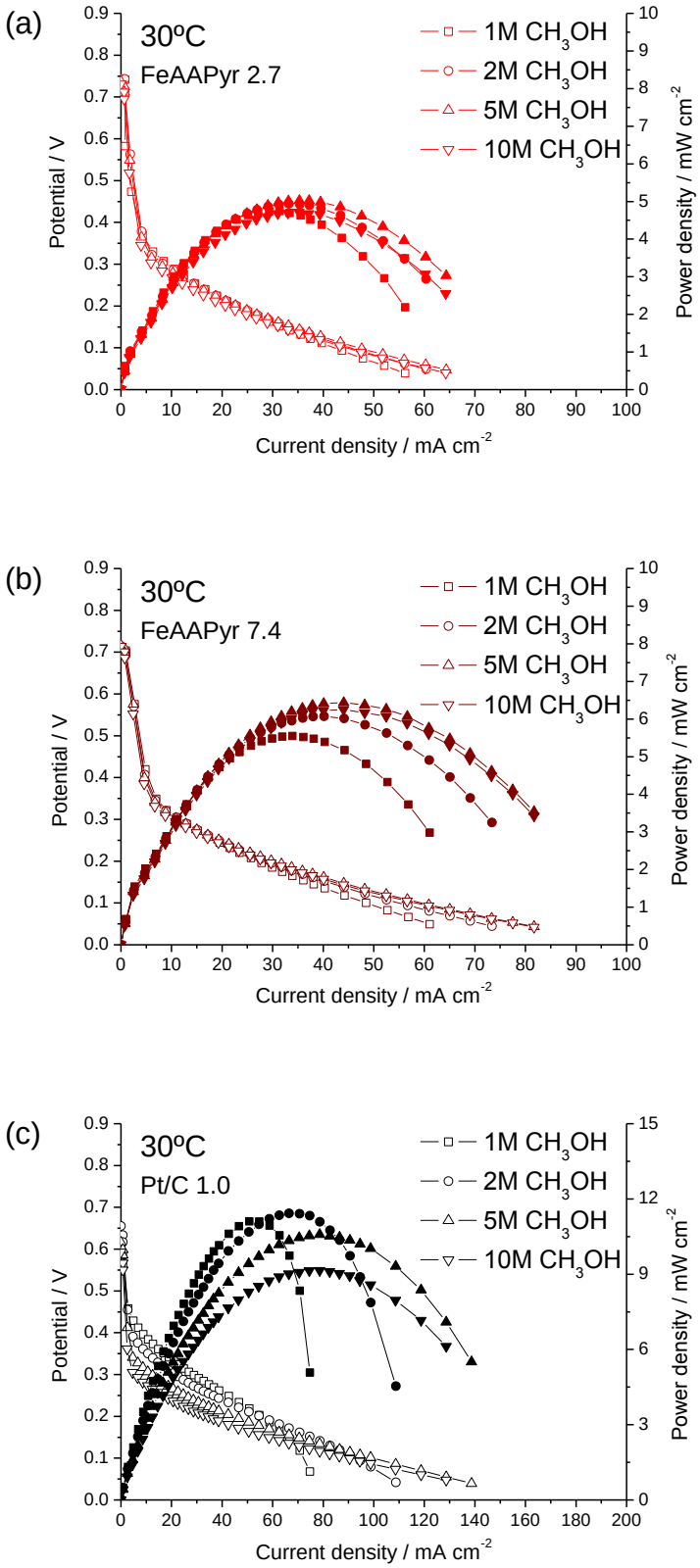
(a)
30ºC
FeAAPyr 2.7
1M CH3OH
2M CH3OH
5M CH3OH
10M CH3OH
Potential / V
Power density / mW cm-2
Current density / mA cm-2
(b)
30ºC
FeAAPyr 7.4
1M CH3OH
2M CH3OH
5M CH3OH
10M CH3OH
Potential / V
Power density / mW cm-2
Current density / mA cm-2
(c)
30ºC
Pt/C 1.0
1M CH3OH
2M CH3OH
5M CH3OH
10M CH3OH
Potential / V
Power density / mW cm-2
Current density / mA cm-2

Figure 4

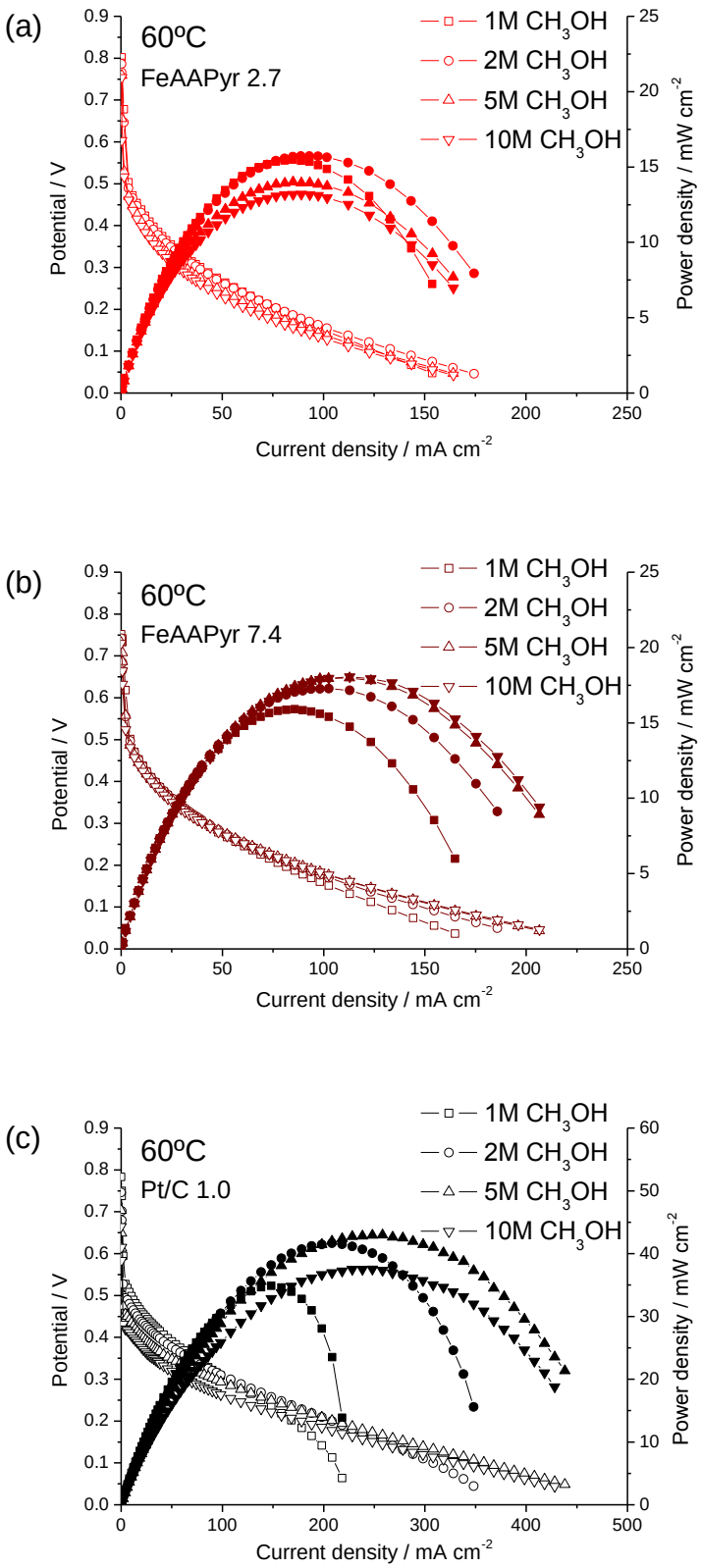
(a)
60ºC
FeAAPyr 2.7
1M CH3OH
2M CH3OH
5M CH3OH
10M CH3OH
Potential / V
Power density / mW cm-2
Current density / mA cm-2
(b)
60ºC
FeAAPyr 7.4
1M CH3OH
2M CH3OH
5M CH3OH
10M CH3OH
Potential / V
Power density / mW cm-2
Current density / mA cm-2
(c)
60ºC
Pt/C 1.0
1M CH3OH
2M CH3OH
5M CH3OH
10M CH3OH
Potential / V
Power density / mW cm-2
Current density / mA cm-2

Figure 5

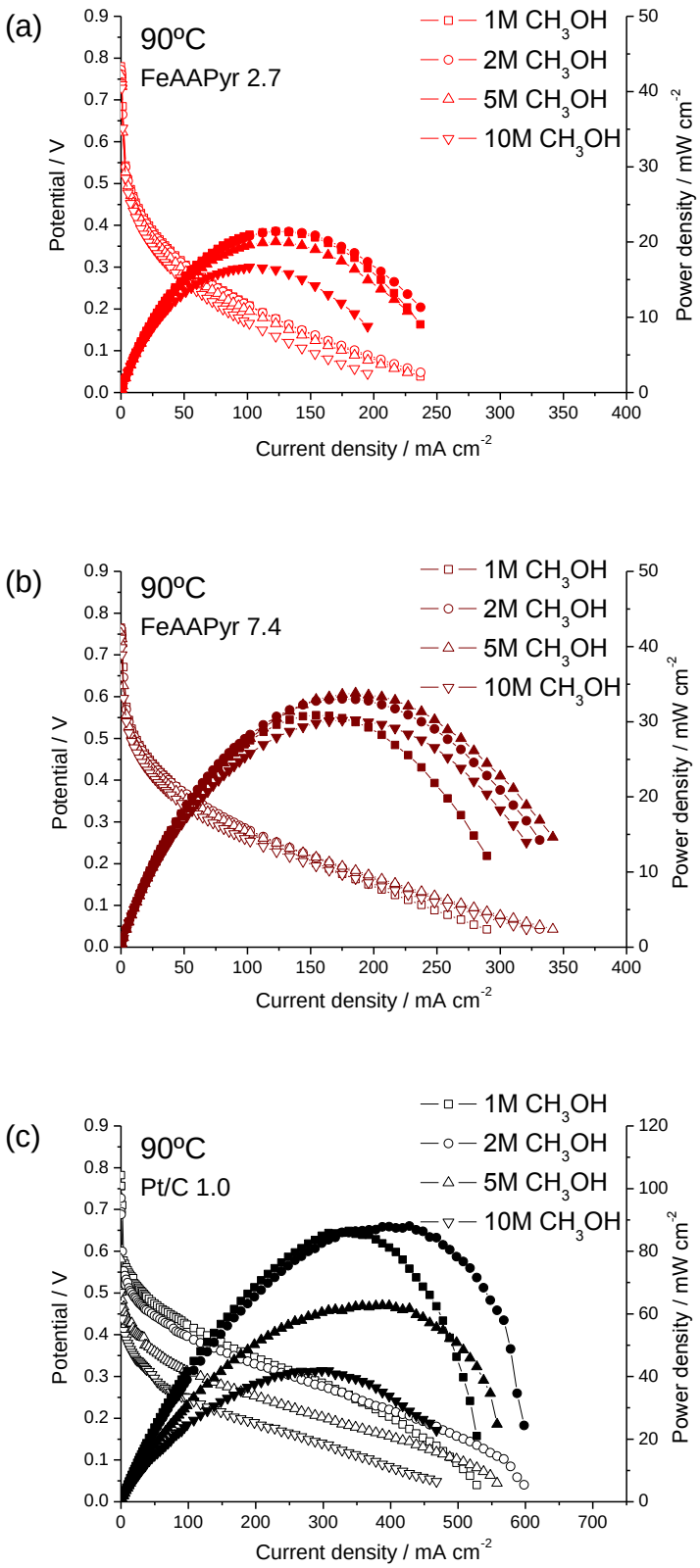
(a)
90ºC
FeAAPyr 2.7
1M CH3OH
2M CH3OH
5M CH3OH
10M CH3OH
Potential / V
Power density / mW cm-2
Current density / mA cm-2
(b)
90ºC
FeAAPyr 7.4
1M CH3OH
2M CH3OH
5M CH3OH
10M CH3OH
Potential / V
Power density / mW cm-2
Current density / mA cm-2
(c)
90ºC
Pt/C 1.0
1M CH3OH
2M CH3OH
5M CH3OH
10M CH3OH
Potential / V
Power density / mW cm-2
Current density / mA cm-2

Figure 6

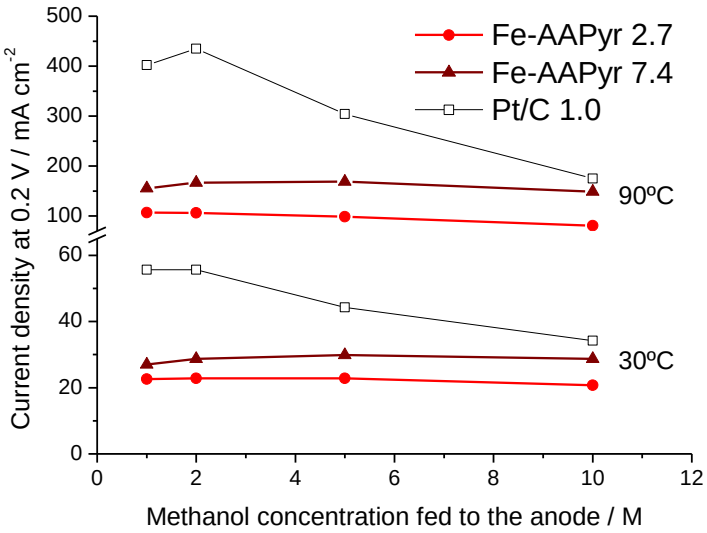
Fe-AAPyr 2.7
Fe-AAPyr 7.4
Pt/C 1.0
90ºC
30ºC
Current density at 0.2 V / mA cm-2
Methanol concentration fed to the anode / M
500
400
300
200
100
60
40
20
0
0
2
4
6
8
10
12

Figure 7

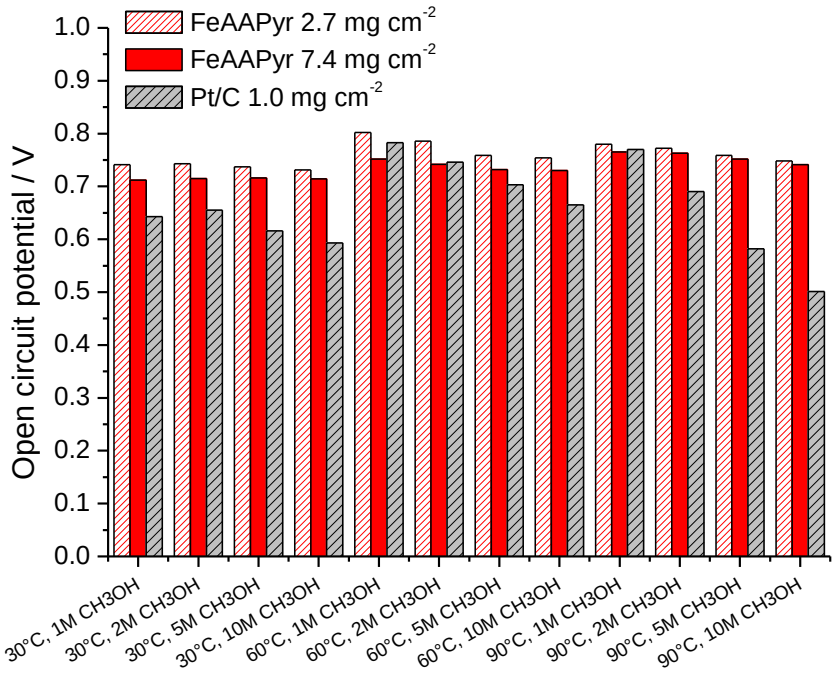
FeAAPyr 2.7 mg cm-2
FeAAPyr 7.4 mg cm-2
Pt/C 1.0 mg cm-2
Open circuit potential / V
1.0
0.9
0.8
0.7
0.6
0.5
0.4
0.3
0.2
0.1
0.0
30°C, 1M CH3OH
30°C, 2M CH3OH
30°C, 5M CH3OH
30°C, 10M CH3OH
60°C, 1M CH3OH
60°C, 2M CH3OH
60°C, 5M CH3OH
60°C, 10M CH3OH
90°C, 1M CH3OH
90°C, 2M CH3OH
90°C, 5M CH3OH
90°C, 10M CH3OH

Figure 8

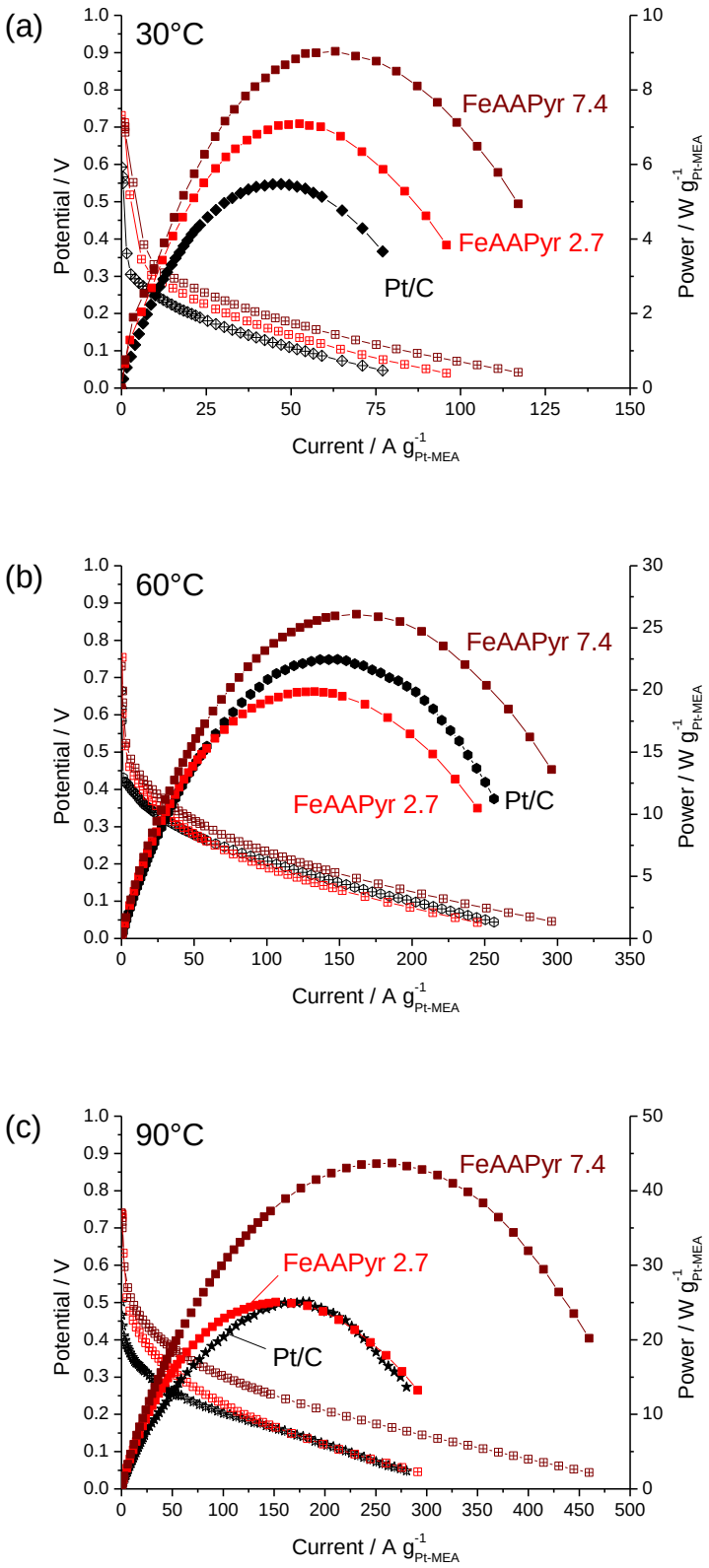
(a)
30°C
FeAAPyr 7.4
FeAAPyr 2.7
Pt/C
Potential / V
Power / W g-1 Pt-MEA
Current / A g-1 Pt-MEA
(b)
60°C
FeAAPyr 7.4
FeAAPyr 2.7
Pt/C
Potential / V
Power / W g-1 Pt-MEA
Current / A g-1 Pt-MEA
(c)
90°C
FeAAPyr 7.4
FeAAPyr 2.7
Pt/C
Potential / V
Power / W g-1 Pt-MEA
Current / A g-1 Pt-MEA

Figure 9

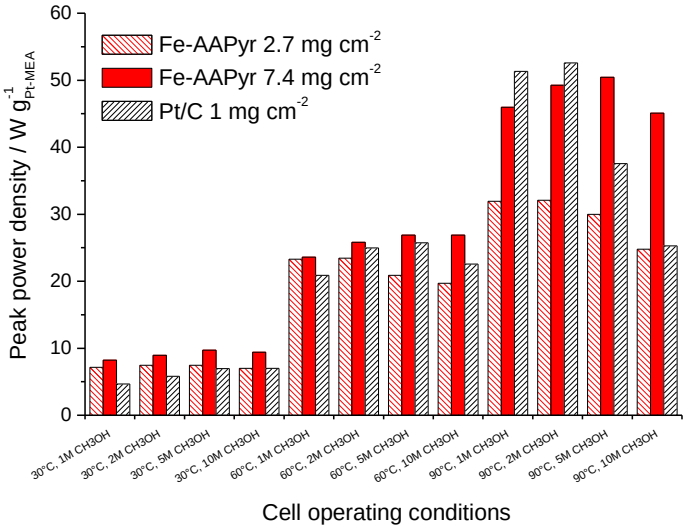
Fe-AAPyr 2.7 mg cm-2
Fe-AAPyr 7.4 mg cm-2
Pt/C 1 mg cm-2
Peak power density / W gPt-MEA-1
0
10
20
30
40
50
60
30°C, 1M CH3OH
30°C, 2M CH3OH
30°C, 5M CH3OH
30°C, 10M CH3OH
60°C, 1M CH3OH
60°C, 2M CH3OH
60°C, 5M CH3OH
60°C, 10M CH3OH
90°C, 1M CH3OH
90°C, 2M CH3OH
90°C, 5M CH3OH
90°C, 10M CH3OH
Cell operating conditions

Figure 10

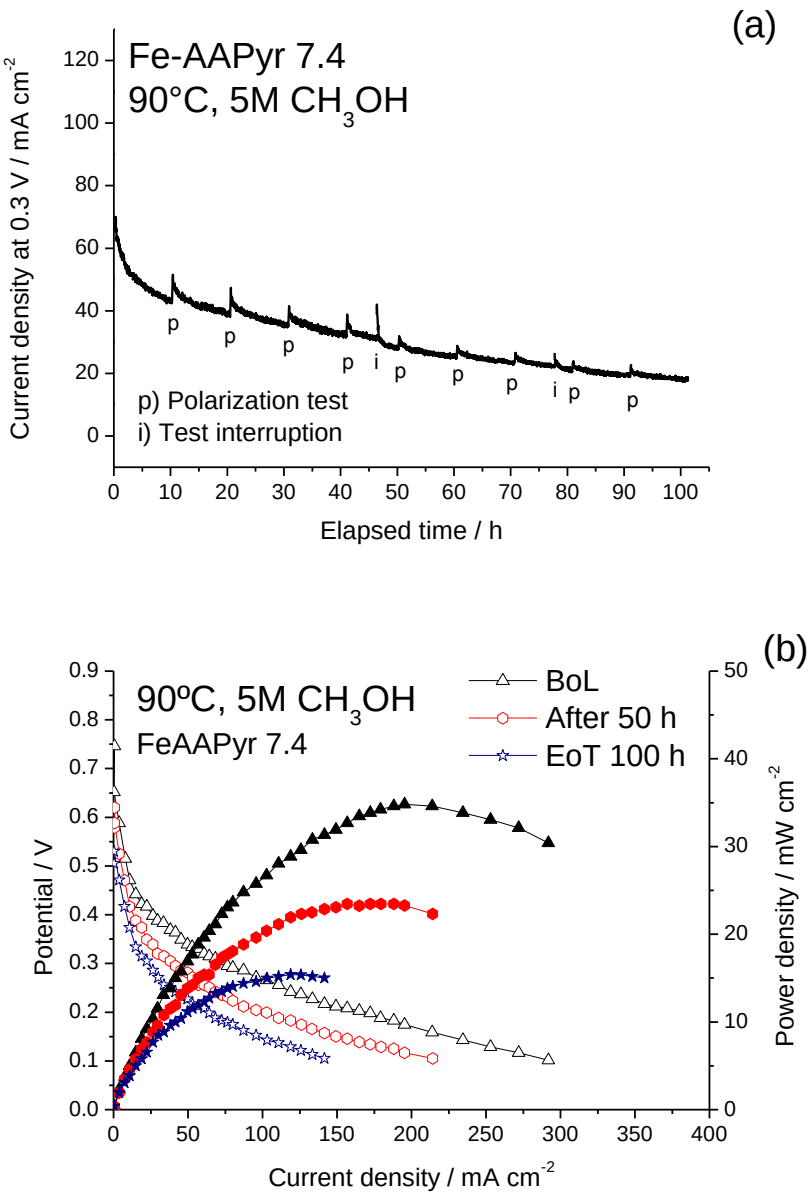
(a)
Fe-AAPyr 7.4
90°C, 5M CH3OH
Current density at 0.3 V / mA cm-2
Elapsed time / h
p) Polarization test
i) Test interruption
(b)
90ºC, 5M CH3OH
FeAAPyr 7.4
BoL
After 50 h
EoT 100 h
Potential / V
Power density / mW cm-2
Current density / mA cm-2

*Graphical Abstract

Graphical Abstract

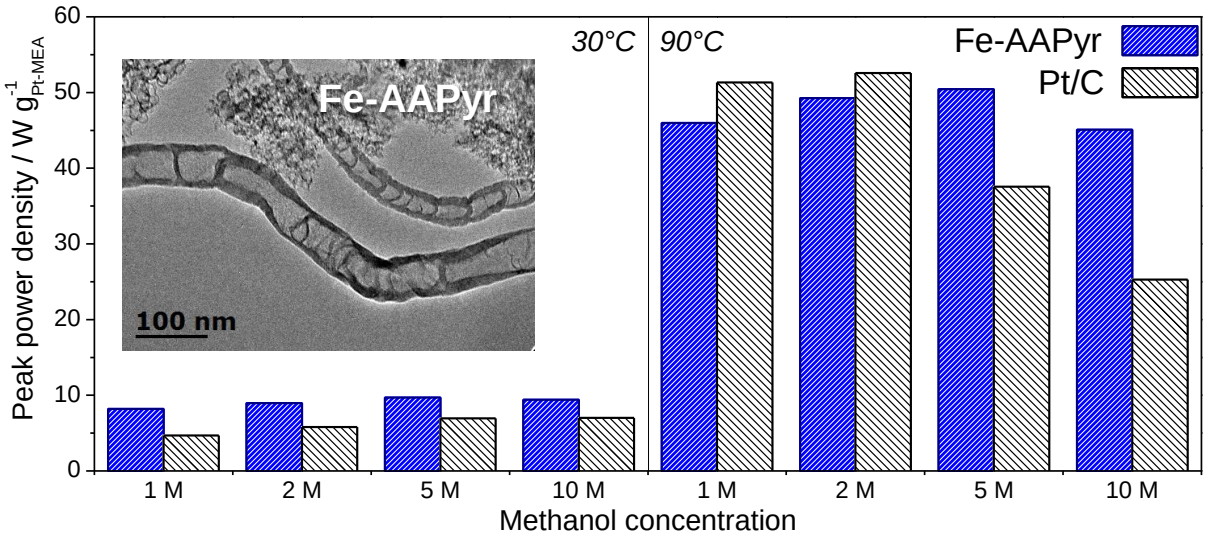

Highlights

- Non-PGM catalyst (Fe-N-C) was synthesized from aminoantipyrine
- First report on PEM-based DMFC performance of such non-PGM catalyst typology
- High ORR activity and remarkable tolerance to the presence of methanol
- High performance of non-PGM catalyst in DMFC even at high methanol concentration